Multiwalled carbon nanotubes dispersed in carminic acid for the development of catalase based biosensor for selective amperometric determination of H_2O_2 and iodate

Arun Prakash Periasamy, Ya-Hui Ho, Shen-Ming Chen *

Department of Chemical Engineering and Biotechnology, National Taipei University of Technology, No. 1, Section 3, Chung-Hsiao East Road, Taipei 106, Taiwan, ROC

ARTICLE INFO

ABSTRACT

We report the preparation of stable dispersion of multiwalled carbon nanotubes (MWCNTs) using carminic acid (CA) as a dispersing agent. The transmission electron microscopy (TEM), scanning electron microscopy (SEM), and atomic force microscopy (AFM) results confirmed that MWCNT is well dispersed in CA aqueous solution and CA has been well adsorbed at MWCNT walls. Fourier transform infrared (FTIR) and UV–vis absorption spectra results also confirmed the adsorption of CA at MWCNT. To develop a highly selective amperometric biosensor for H_2O_2 and iodate, the model enzyme catalase (CAT) was immobilized at CACNT modified glassy carbon electrode surface. The immobilized CAT exhibits well defined quasi reversible redox peaks at a formal potential ($E^{\circ\prime}$) of -0.559 V in 0.05 M pH 7 phosphate buffer solution (PBS). The proposed CAT/CACNT biosensor exhibits excellent amperometric response towards H_2O_2 and iodate in the linear concentration range between 10 μM to 3.2 mM and 0.01–2.16 mM. The sensitivity values are 287.98 μA mM^{-1} cm^{-2} and 0.253 mA mM^{-1} cm^{-2}, respectively. Moreover, the developed CAT biosensor exhibits high affinity for H_2O_2 and iodate with good selectivity.

© 2011 Elsevier B.V. All rights reserved.

1. Introduction

Hydrogen peroxide (H_2O_2) is an essential component of plant tissues, which regulates the plant metabolism, defense, acclimatory processes and gene expression (Slesak et al., 2007). Moreover, H_2O_2 has excellent oxidizing and antibacterial property and it has been widely employed in industries as an oxidizing agent (Yeh et al., 2003), antibacterial agent (Weston, 2000) and bleaching agent (Moore and Argyropoulos, 1999). Owing to the critical role played by H_2O_2 in biological systems as well as its wide applications in diverse fields, it has been extensively studied these days. On the other hand, iodine is the most vital micronutrient which is obligatory for the well-being of all individuals. In recent years, iodine deficiency is a worldwide reported serious health problem and it impersonates solemn threats to all stages of human life. Predominantly, in pregnant woman its deficiency leads to cretinism and in the case of older children and adolescents the temporary iodine insufficiency causes reduced physical and academic performance (Ketpichainarong et al., 2010). Nevertheless, one of the main factors accountable to iodine deficiency is the dietary inadequacy of

iodine. To date the most suitable method to avoid iodine deficiency is fortification of salt with iodine (Ahad and Ganie, 2010).

It is exigent to achieve sensitive H_2O_2 and iodate determinations in routine analysis by the existing conventional approaches (Matsubara et al., 1985; Jackson and Hewitt, 1996; Kazuaki, 1997; Bichsel and Gunten, 1999; Zarei, 2009). Hence, there has been colossal demand for developing novel H_2O_2 and iodate quantification methods with simple and cost-effective measurement protocols. Conversely, by employing versatile electrochemical techniques in concert with the implementation of enzyme based biosensors highly sensitive H_2O_2 and iodate quantifications have been achieved these days (Salimi et al., 2007a). Catalase (CAT) is an active enzyme of oxidoreductase family which catalyzes the disproportionation process of H_2O_2 and it has been widely employed in H_2O_2 based biosensors (Prakash et al., 2009a). Multiwalled carbon nanotubes (MWCNTs) with their exceptional stability, good electrical conductivity and high mechanical strength (Srivastava and Wei, 2003) have been used as compelling immobilization matrices for CAT to accomplish sensitive H_2O_2 detection and for promoting the direct electron transfer of CAT (Prakash et al., 2009a). Earlier, we reported the direct electrochemistry of CAT at nafion (NF) wrapped MWCNTs in the presence of didodecyldimethylammonium bromide (DDAB) through electrostatic interactions between CAT, MWCNT-NF and DDAB (Prakash et al., 2009b).

* Corresponding author. Tel.: +886 2270 17147; fax: +886 2270 25238.
E-mail address: smchen78@ms15.hinet.net (S.-M. Chen).

On the other hand, because of the hydrophobic nature and Van der Waals attractions between the nanotubes, it is always difficult to prepare stable aqueous dispersion of MWCNTs. This imperative shortcoming necessitates the need for exploring novel dispersing agents with versatile strategies (Kharisov et al., 2009). The most widely employed strategy is the attachment of functional groups at MWCNT walls through covalent and noncovalent approaches (Tasis et al., 2006). Even if stable MWCNT dispersion could be prepared by acid treatment, larger agglomerates and longer tubes with poorer graphene layers will break at a highest rate during acid treatment (Wang et al., 2003). To avoid this, in majority of the cases noncovalent approach has been preferred. The dispersing agents often used in noncovalent approach are surfactants (Madni et al., 2010), polymers (Liu et al., 2006), DNA (Li et al., 2009a) and biomolecules (Moulton et al., 2005). However, several parameters including surfactants/monomer concentrations and compatibility of the biomolecules have to be optimized. Especially, storage stability of the MWCNT dispersions prepared by the above stated methods are of great concern, when biomolecules are used as dispersing agents. Alternatively, by using simple ultrasonication treatments stable dispersion of MWCNT can be prepared by dispersing them in organic dyes through strong π-π stacking interactions. Besides, this kind of strategy is simple, economical, color variations of dye solutions could be visually observed and the MWCNT-dye adducts formed could be confirmed by several available spectroscopic and surface morphological studies (Zhang and Silva, 2010).

Carminic acid (7-D-glucopyranosyl-3,5,6,8-tetrahydroxy-1-methyl-9,10-dioxo-9,10-dihydroanthracene-2-carboxylic acid or CA), is the active color ingredient of natural dye cochineal produced by *Dactylopius coccus*, a cochineal insect (Gaweda et al., 2008). As shown in Fig. S1, structure of CA possesses an anthraquinone moiety linked to glucose sugar unit. CA is non-toxic, possess antitumor and antioxidant property (Li et al., 2009b), and used as a coloring agent in various food stuffs (Lancaster and Lawrence, 1996). Moreover, CA shows good biocompatibility for various proteins and it undergoes strong interactions with biomolecules (Sun et al., 2006). Besides, CA is a compound of great electrochemical importance. Several reports about the electrochemical (Grygar et al., 2003; Carbo et al., 2003), impedance behavior (Rashwan, 2005) and spectroscopic analysis (Rasimas and Blanchard, 1995; Canamares et al., 2006) of CA are available in literature.

However, to the best of our knowledge no reports are available about the preparation of stable aqueous dispersion of MWCNT using CA as a dispersing agent. Moreover, CA functionalized MWCNT have not been used as an immobilization platform for CAT. In this work, we adapted a noncovalent approach with simple ultrasonication treatment for preparing more stable aqueous dispersion of MWCNT using CA as a dispersing agent. The π-π stacking interactions between CA and MWCNTs provide good stability to the CACNT dispersion. We utilized the prepared CACNTs as a novel matrix for CAT immobilization and to explore its direct electrochemistry. CAT immobilized at CACNT modified electrode shows good affinity and high selectivity towards H_2O_2 and iodate with appreciable sensitivity.

2. Experimental

2.1. Reagents

Carminic acid was purchased from Sigma–Aldrich. MWCNT with O.D. 10–15 nm, I.D. 2–6 nm and length 0.1–10 μm was obtained from Aldrich. CAT from bovine liver (4540 units mg^{-1}) was purchased from Sigma. H_2O_2 (30%) and potassium iodate were obtained from Wako Pure Chemical Industries, Ltd. The supporting

electrolyte used for all experiments is 0.05 M pH 7 phosphate buffer solution (PBS). All aqueous solutions were prepared using doubly distilled water. Prior to each experiment, the solutions were deoxygenated with pre-purified N_2 gas for 10 min and N_2 tube was kept above the solutions to maintain an inert atmosphere.

2.2. Apparatus

Cyclic voltammetry experiments were carried out using CHI 1205a work station. GCE with an electrode surface area of 0.079 cm^2 was used as working electrode. Pt wire with 0.5 mm diameter was used as counter electrode and standard Ag/AgCl was used as a reference electrode. Amperometry studies were performed using CHI 750 potentiostat with analytical rotator AFMSRX (PINE Instruments, USA). UV–vis absorption and fourier transform infrared (FTIR) spectroscopy measurements were carried out using Hitachi U-3300 spectrophotometer and Perkin Elmer spectrum RXI. EIM6ex ZAHNER (Kroanch, Germany) was used for electrochemical impedance spectroscopy (EIS) studies. Surface morphology studies were performed using JEM 2007 model transmission electron microscope (TEM), Hitachi S-3000 H scanning electron microscope (SEM) and Being nano-instruments CSPM 4000, atomic force microscope (AFM).

2.3. Preparation of CACNTs

About 10 mg of MWCNT was added into 10 ml of 5 mM CA aqueous solution and the whole mixture was ultrasonicated for 1 h, until a homogeneous slight reddish-black dispersion was obtained. CACNT dispersion was then filtered and the solid material was subjected to several washings with water and over night dried at 50 °C in an air oven. Thus obtained CACNTs were dissolved in aliquots of double distilled water and sonicated well to obtain a final concentration of 1 mg ml^{-1}. For comparison, without any CA addition 1 mg of as-received MWCNT was dispersed in 1 ml of doubly distilled water and sonicated well. Hereafter, the term CNT used elsewhere in this paper will represent the non-functionalized MWCNT-water dispersion.

3. Results and discussion

3.1. Investigation of long term storage stability and surface morphological characterizations

In order to evaluate the long term storage stability, prepared CACNT and CNT dispersions were stored in two separate small micro centrifuge tubes, kept at room temperature and were examined regularly. The photographs taken at various intervals are shown in Fig. 1(a–m). No notable precipitation of nanotubes bundles was observed in CACNT dispersion even after four months (see Fig. 1(m)). This result validates the good storage stability of CACNT dispersion and it could be ascribed to the strong π-π interactions between MWCNT walls and CA. In contrast, CNT dispersion displayed poor storage stability, where CNT bundles precipitated completely after 1 month (see Fig. 1(j)). The poor storage stability of CNT dispersion can be ascribed to the hydrophobic nature and strong Van der Waals attractions between the individual nanotubes.

The surface morphology of prepared CNT and CACNT dispersions were comparatively studied using TEM. As shown in Fig. 1A, TEM image of CNT dispersion shows few well defined CNTs with an O.D. of 10 nm. The black spots found at CNT walls might be the metal catalyst impurities. However, in the TEM image of CNT took at higher magnifications more agglomerates were found (figure not shown). Whereas, as shown in Fig. 1(B–D), TEM images of CACNT dispersion took at 20 nm and 5 nm magnifications displays the well dispersed
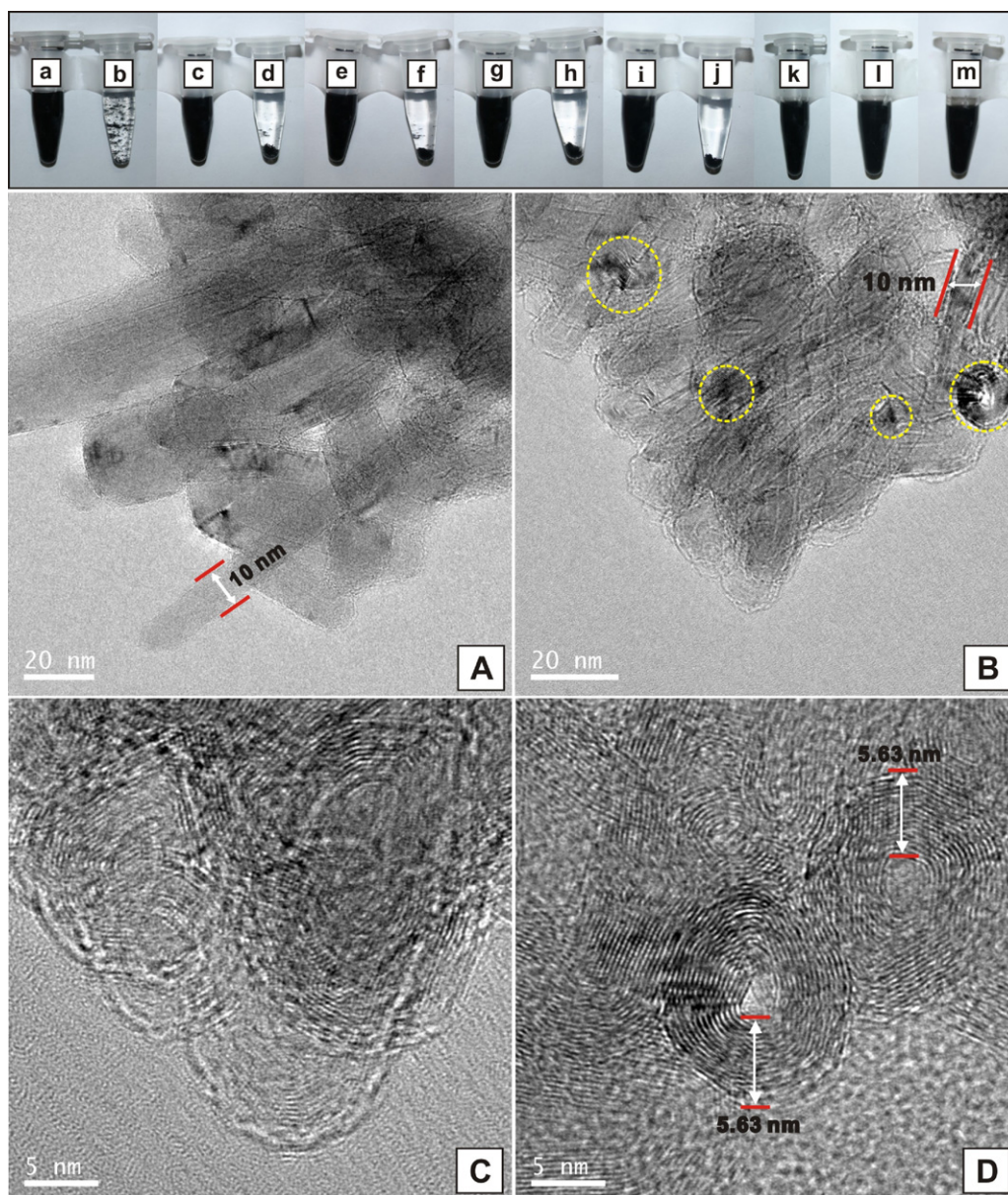
Fig. 1. Photographs of: 1 mg ml^{-1} of CACNT dispersion took after (a) 1 h, (c) 1, (e) 2, and (g) 3 weeks; (i) 1, (k) 2, (l) 3, and (m) 4 months; CNT dispersion took after: (b) 1 h, (d) 1, (f) 2, and (h) 3 weeks; (j) 1 month. TEM images of (A) CNT and (B–D) CACNT at different magnifications. (B) The dotted circles in yellow color indicate the adsorbed CA molecules. The arrows in: (A) and (D) indicate the O.D. and I.D. of CNT and CACNTs. (For interpretation of the references to color in this figure legend, the reader is referred to the web version of the article.)

CACNTs with extended nano-tubular structures. As indicated by arrows in Fig. 1B, O.D. of CACNT is about 10 nm. The dotted circles in yellow color indicate the CA molecules adsorbed at MWCNT walls. Similarly, close view of CACNT presented in Fig. 1(C) and (D) confirmed the adsorption of CA at the nanotube walls. As indicated by arrows in Fig. 1D, CACNTs possess coiled structures with 5.63 nm diameter, which is close to the prescribed I.D. of MWCNTs used in this work. TEM results confirmed that CACNTs retain their native surface morphology even after functionalization with CA.

3.2. CAT immobilization and surface morphological characterization using SEM and AFM studies

About 10 μl of CACNT dispersion was drop casted on a pre-cleaned GCE surface and dried at 30 °C in an air oven for 30 min. CACNT modified GCE was gently washed few times with doubly distilled water and transferred to an electrochemical cell containing 5 mg ml^{-1} CAT solution. As shown in Fig. S2, 15 consecutive cyclic voltammograms (CVs) were recorded at the scan rate of 50 mV s^{-1} in the potential range between −0.1 and −0.9 V to obtain stable voltammograms. CAT/CACNT/GCE was then washed gently with doubly distilled water and dried at 30 °C. Each time, 5 consecutive cycles were recorded at CAT/CACNT/GCE in PBS to remove the loosely adsorbed CAT molecules. The prepared CAT/CACNT/GCE was stored in PBS at 4 °C when not in use. For comparison, only CACNT/GCE was also prepared.

Surface morphology of all the prepared films was investigated using SEM. Fig. S3A shows the SEM image of CNT film. Here, the CNT bundles are flocked together and more closely distributed throughout the CNT film surface, which reveals the poor dispersing ability of CNT in water. Whereas Fig. S3B shows the SEM image of CACNT film which possesses more homogeneous and well-dispersed CAC-NTs. No notable CACNT agglomerates were found. Fig. S3C shows the SEM image of CAT film surface which contains several bright
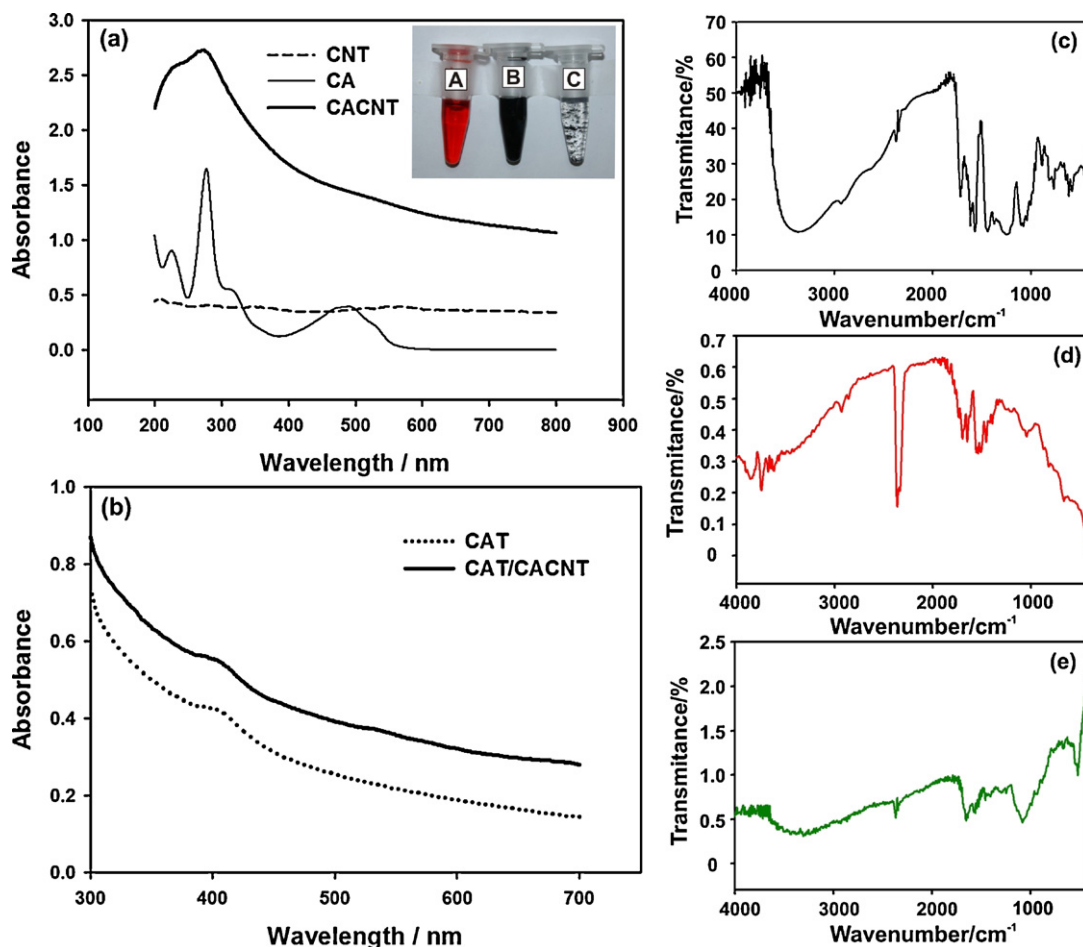
Fig. 2. (a) UV–vis absorption spectra of CNT (dashed line), CA (thin line) and CACNT (bold line) aqueous dispersions. Inset is the photograph of (A) CA, (B) CACNT, and (C) CNT aqueous dispersions. (b) UV–vis absorption spectra of 5 mg ml^{-1} of CAT solution (dotted line) and CAT/CACNT mixture (bold line). The FTIR spectra: of (c) CA, (d) CACNT and (e) CAT/CACNT.

cotton bolls like structures. While Fig. S3D displays the uniform surface morphology of CAT/CACNT film. Here, the bright cotton bolls like structures of CAT are not clearly seen. Instead a thin, uniform CAT film covering the entire CACNT film surface is observed which authenticates the good affinity of CAT molecules towards CACNT. The above mentioned SEM results provide evidence for the formation of CAT/CACNT film, validating CACNT as a suitable matrix for CAT immobilization. The AFM results also showed that bright cotton bolls like structure of CAT has been efficiently immobilized at CACNTs and the composite film possess smooth surface morphology (see Fig. S4).

3.3. UV–vis absorption and FTIR spectroscopic studies

UV–vis absorption spectroscopy study has been used to confirm the functionalization of CA at MWCNT walls and to ensure whether CAT retains its native structure at CACNT. Fig. 2(a) shows the UV–vis absorption spectra of CNT, CA and CACNT aqueous dispersions. In Fig. 2 inset, (A)–(C) represent the capped micro centrifuge tubes containing CA (red color), CACNT (black), and CNT aqueous dispersions, in which CACNT dispersion looks homogenous and well dispersed than CNT dispersion. No characteristic absorption bands were observed in the absorption spectra of CNT aqueous solution. However, in the same wavelength range CA aqueous solution exhibits two sharp absorption peaks at 225, 277 nm and two broader peaks at 315 nm and 490 nm. In particular, the

absorbance maximum noticed at 490 nm for CA aqueous solution is close to the absorbance maximum of 492 ± 1 nm for 1×10^{-5} M CA aqueous solution (Canamares et al., 2006). Similar to the CA absorption bands at 225 and 277 nm, CACNT also displayed two slightly blunted absorption bands at same wavelength. However, CA absorption bands found at 315 nm and 490 nm were absent in the absorption spectra of CACNT, which might have shifted due to the association of CA with MWCNT. UV–vis absorption spectroscopy results thus confirm the functionalization of CA at MWCNT walls. UV–vis absorption spectra of native CAT solution exhibit a soret band at 407 nm (Shima et al., 2001). As shown in Fig. 2(b), both native CAT solution (dotted line) and CAT/CACNT mixture (bold line) displayed similar soret bands at 406 nm, which indicated that incorporation of CAT with CACNT does not affect the native structure of CAT and it remains stable in the CACNT microenvironment.

From the FTIR spectra of CA shown in Fig. 2(c), the frequencies in wavenumber (cm^{-1}) and band assignments are obtained and they are given in Table S1. It is clear from Table S1 that, majority of the absorption bands of CA reported in this work are in good agreement with the CA absorption bands reported by Canamares et al. (2006). Fig. 2(d) and (e) shows the FTIR spectra of CACNT and CAT/CACNT. Compared with the FTIR spectra of CA, FTIR spectra of CACNT and CAT/CACNT also exhibits characteristic CA absorption bands at 3359, 2931, 1649, 1565, 1258 and 1078 cm^{-1}, which confirmed that both CACNT and CAT/CACNT are functionalized with CA. The CAT molecules should retain their native structure at CACNT
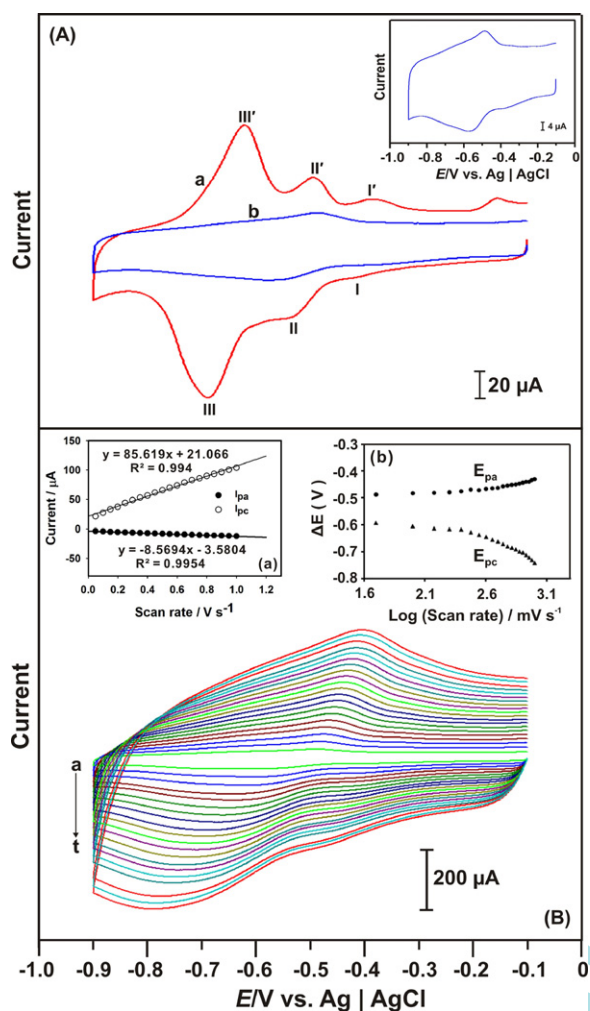
Fig. 3. (A) CVs of (a) CACNT and (b) CAT/CACNT film modified GCEs obtained at the scan rate of $50 \, mV \, s^{-1}$. Inset is the enlarged view of (b). (B) CVs obtained at CAT/CACNT/GCE at different scan rates. Scan rates from (a–t) are 50, 100, 150, 200, 250, 300, 350, 400, 450, 500, 550, 600, 650, 700, 750, 800, 850, 900, 950 and $1000 \, mV \, s^{-1}$ respectively. Supporting electrolyte: N_2 saturated PBS. The inset plots are (a) the peak currents (I_{pa} and I_{pc}) vs. scan rate/$V \, s^{-1}$ and (b) variation of peak potential vs. log (scan rates).

film since the association of CAT with CACNT does not produce any shift in CA absorption bands.

3.4. Investigation of direct electrochemistry of CAT using cyclic voltammetry

Fig. 3A shows the CVs obtained at CACNT and CAT/CACNT film modified GCEs in N_2 saturated PBS at the scan rate of $50 \, mV \, s^{-1}$. CACNT modified GCE exhibits three well defined redox couples (I–I′, II–II′ and III–III′) with maximum cathodic and anodic peak currents (I_{pc} and I_{pa}). The formal potential ($E^{\circ\prime}$) values for these redox couples are $-0.400 \, V$, $-0.512 \, V$ and $-0.654 \, V$, respectively. Similar electrochemical behavior has been reported at anthraquinone modified CNT electrodes (Kumar and Swetha, 2011). The redox peaks observed at positive potential are smaller than those observed at more negative potentials and hence there may not be possibility for the hydroquinone formation via consecutive one electron step. Instead they believe that voltammetric peaks appearing at different potentials might have resulted from the multiple site adsorptions of anthraquinone on inner and outer walls of MWCNTs and as they own different adsorption energies. Similarly, in the present study as evident from the TEM results discussed

in Fig. 1(B–D), due to the adsorption of CA at the inner and outer walls of MWCNT the peaks (II–II′) and (III–III′) might have appeared. However, the small ill-defined redox peaks (I–I′) found at more positive potential might be due to the formation of the intermediate reduction/oxidation of the quinine/semiquinone species (Heald et al., 2004). Compared with CACNT/GCE, CAT/CACNT/GCE exhibits single well-defined quasi reversible redox peaks with smaller peak currents, which may be due to the interaction between CACNT and the immobilized CAT molecules. Sun et al. reported similar voltammetric behavior for the interaction between CA and human serum albumin (Sun et al., 2006). Fig. 3A inset shows the enlarged view of cyclic voltammogram obtained at CAT/CACNT/GCE. Unlike CACNT/GCE, CAT/CACNT/GCE exhibits a single well-defined redox couple at an E° value of $-0.523 \, V$. This $E^{\circ\prime}$ value is slightly more negative than the $E^{\circ\prime}$ value reported at other CAT modified electrodes (Lu et al., 2007; Shen and Hu, 2005; Vatsyayan et al., 2010). The formal potential shifts observed at CAT based electrodes could be due to the interaction of various film components with CAT or by their effect on electrical double layer (Shen and Hu, 2004).

Fig. 3B shows the CVs obtained at CAT/CANT/GCE in N_2 saturated PBS at different scan rates. Inset (a) in Fig. 3B shows the peak currents (I_{pa} and I_{pc}) vs. scan rates plot which exhibits a linear relationship with $R^2 = 0.9940$ and 0.9954, indicating a surface-confined redox process. Inset (b) in Fig. 3B shows the linear dependence of change in peak potentials over logarithm of scan rates. From the slope values of ΔE vs. log (scan rates), by assuming the value of $\alpha \approx 0.5$ and number of electrons transferred for $Fe^{(III/II)}$ redox process of CAT as one, the electron transfer rate constant (k_s) has been calculated using Laviron theory (Laviron, 1979). The k_s value of CAT at CAT/CACNT/GCE is estimated to be $1.22 \, s^{-1}$, which is close to the k_s values reported at other CAT modified electrodes (Wang et al., 2007; Salimi et al., 2005, 2007b; Zhou et al., 2008; Vatsyayan et al., 2010). Thus CACNT have augmented the electron transfer process of CAT. Further, the surface coverage concentration (Γ) value of CAT at CAT/CACNT/GCE is calculated as $1.49 \times 10^{-9} \, mol \, cm^{-2}$, which is higher than the Γ value of CAT reported at other MWCNT modified electrodes (Prakash et al., 2009b; Salimi et al., 2007a). This can be attributed to the larger surface area of CACNT which helps for more efficient CAT immobilization. Fig. S5 shows the effect of pH on the redox behavior of CAT/CACNT/GCE in various pH solutions. The redox couple observed at CAT/CACNT is stable in the pH range between 4 and 11 and the redox process involves equal number of proton and electron transfer process (see supplementary data).

3.5. EIS and electrocatalytic H_2O_2 and iodate reduction studies

Fig. 4A shows the real and imaginary parts of impedance spectra represented as Nyquist plots (Z_{im} vs. Z_{re}) for bare/GCE, CACNT and CAT/CACNT film modified GCEs. Nyquist plot of CAT/GCE obtained under similar conditions is shown in the inset (see inset (a) in Fig. 4A). The Randles equivalence circuit model is also shown in Fig. 4A inset. Interestingly, Nyquist plot of CAT/GCE displays an enlarged semicircle with highest R_{et} value of $1.614 \, K\Omega$, representing the electron transfer-limited process. Compared with CAT/GCE, bare/GCE exhibits a much smaller semicircle with a R_{et} value of $157.4 \, \Omega$, validating a rapid electron transfer process at the later. However, no semicircles were observed in the Nyquist plot of both CACNT and CAT/CACNT/GCEs, instead they exhibit straight lines, indicating a diffusion-limited process. The R_{et} values of CACNT and CAT/CACNT/GCEs are about $4.854 \, \Omega$ and $6.717 \, \Omega$, which are comparatively lower than R_{et} values of CAT and bare GCEs, validating faster electron transfer kinetics at the CACNT modified electrodes. This can be ascribed to the excellent conductivity of CACNT.

Fig. 4B shows the CVs obtained at CAT/CACNT film modified GCE in the absence and presence of various H_2O_2 concentrations. In the presence of H_2O_2, CAT/CACNT modified GCE exhibits a
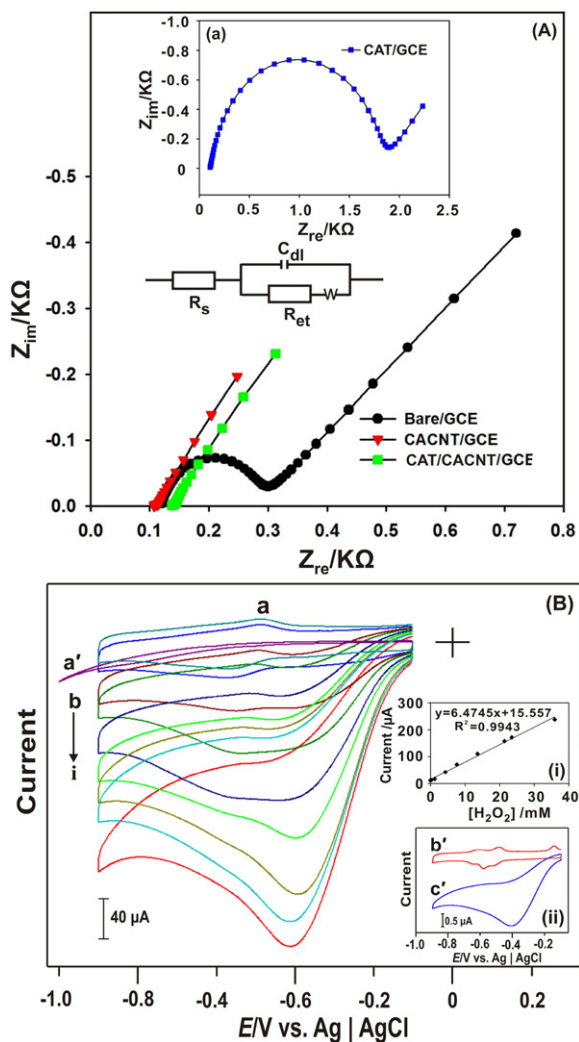
Fig. 4. (A) EIS of bare, CACNT and CAT/CACNT film modified GCEs in PBS containing 5 mM $Fe(CN)_6^{3-}/Fe(CN)_6^{4-}$. (a) EIS of CAT/GCE; Randles equivalence circuit used for fitting EIS data is also shown in the inset. Amplitude: 5 mV, frequency: 100 mHz to 100 kHz. (B) CVs obtained at CAT/CACNT/GCE in the absence (a) and presence of: (b) 0.25, (c) 1.23, (d) 4.31, (e) 7.62, (f) 13.6, (g) 21.4, (h) 23.5, and (i) 36 mM H_2O_2; (a′) bare GCE in 36 mM H_2O_2. Inset (i) plot of I_{pc} vs. $[H_2O_2]$. Inset (ii) CVs of CACNT (b′) and CAT/CACNT/GCEs (c′) in 36 mM of H_2O_2.

reduction peak at −0.4 V. Upon increase in H_2O_2 concentrations, the cathodic peak currents increased while anodic peak currents decreased, where, both the increase in peak current and decrease in over potential are considered as electrocatalysis. Comparing curve (i) with (a′) in Fig. 4B, the enhanced reduction peak observed at CAT/CACNT/GCE for 36 mM H_2O_2 shows its excellent electrocatalytic activity towards H_2O_2, while the absence of reduction peak at bare/GCE showed it poor electrocatalytic activity. The linear regression equation was obtained as I (μA) = 6.4745C (mM) + 15.557, R^2 = 0.9943 (Inset (i) in Fig. 4B). The linear H_2O_2 concentration range and sensitivity values are 4.31–36 mM and 81.96 μA mM^{-1} cm^{-2}. Further, the electrocatalytic activity of CAT/CACNT/GCE is higher than the electrocatalytic activity of CACNT/GCE (Inset (ii) in Fig. 4B). The excellent electrocatalytic activity of the composite film towards H_2O_2 could be ascribed to the synergistic effect of CACNT for H_2O_2, biocompatibility of immobilized CAT and the ability of CA to mediate electrocatalytic process (Ardakani et al., 2010). Fig. S6 shows the schematic representation of electrocatalytic H_2O_2 reduction process occurring at CAT/CACNT/GCE mediated by CA, in which the quinone moiety present in CA could be reduced to hydroquinone. The effect of temperature on the electrocatalytic

activity of CAT/CACNT film towards 25 mM H_2O_2 has also been investigated in N_2 saturated PBS and the results are shown in Fig. S7. The optimum working temperature for this CAT biosensor is 30 °C. Fig. S8 shows the electrocatalytic responses observed at CAT/CACNT/GCE for various iodate concentrations. The I_{pc} observed at CAT/CACNT/GCE increased linearly with increase in iodate concentrations between 1.67 and 14 mM. The linear regression equation is I (μA) = 4.615C (mM) + 32.73, R^2 = 0.9953 (Fig. S8 inset). The sensitivity value is 58.42 μA mM^{-1} cm^{-2} (see supplementary data). The mechanism for the reduction of IO_3^- to I^- at CAT film surface can be explained by the following equations (Salimi et al., 2007a).

$$6\,\text{Catalase Fe}^{III}(\text{oxidized form}) + 6e^-$$
$$\rightarrow 6\,\text{Catalase Fe}^{II}(\text{reduced form}) \tag{1}$$

$$6\,\text{Catalase Fe}^{II}(\text{reduced form}) + IO_3^- + 6H^+$$
$$\xrightarrow{K_{cat}} 6\,\text{Catalase Fe}^{III}(\text{oxidized form}) + I^- + 3H_2O \tag{2}$$
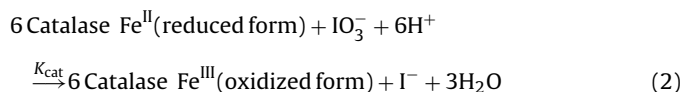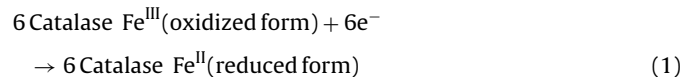
3.6. Amperometric determination of H_2O_2 and iodate at CAT/CACNT film modified rotating disc glassy carbon electrode

Fig. 5A displays the amperogram obtained at CAT/CACNT film modified rotating disc glassy carbon electrode (RDE) in N_2

Fig. 5. (A) Amperometric response at CAT/CACNT modified RDE upon the addition of 1 μM to 5.8 mM H_2O_2; applied potential: −0.4 V, the inset (a) response current vs. $[H_2O_2]$ plot, (b) linear calibration plot and (c) Linweaver–Burk plot used for K_M^{app} determination, (B) amperometric response at CAT/CACNT modified RDE upon the addition of 0.01–2.16 mM IO_3^-; applied potential: −0.75 V. The insets are: (a) the linear calibration plot and (b) Linweaver–Burk plot used for K_M^{app} determination. Supporting electrolyte: N_2 saturated PBS; rotation rate: 1200 rpm.

saturated PBS for various H_2O_2 concentration additions. CAT/CACNT film exhibits steady, well defined amperometric response towards H_2O_2 within 5 s. Inset (a) in Fig. 5A shows the linear dependence of response current on various H_2O_2 concentrations. From the calibration plot, linear H_2O_2 concentration range and sensitivity values are obtained as 10 μM to 3.2 mM and 287.98 μA mM^{-1} cm^{-2} (inset (b) in Fig. 5A). The linear regression equation is I (μA) = 69.115C (mM) + 21.483, R^2 = 0.9895. The response curve exhibits a Michaelis–Menten behavior after 3000 s for 4 mM H_2O_2 concentration additions and it approaches a plateau after the addition of 6 mM H_2O_2. This indicates that enzyme activity has attained its saturation level at such high substrate concentrations. In order to study the enzyme kinetics as well as to evaluate the affinity of immobilized CAT towards H_2O_2, Michaelis–Menten constant (K_M^{app}) has been calculated from the electrochemical version of the Lineweaver–Burk equation shown in Eq. (3) (Kamin and Willson, 1980).

$$\frac{1}{I_{ss}} = \frac{1}{I_{max}} + \frac{K_M^{app}}{I_{max}} \frac{1}{C} \tag{3}$$

In the above equation, I_{ss} represents the steady state current measured after the addition of substrate, I_{max} is the maximum current measured under saturated substrate concentration, and C is the bulk concentration of substrate. From the plot of $1/I_{ss}$ vs. $1/C$, the slope (K_M^{app}/I_{max}) and intercept ($1/I_{max}$) values are obtained as 0.0031 and 0.0146. The I_{max} and K_M^{app} values are calculated as 68.49 and 0.21 mM, respectively. The K_M^{app} value observed at CAT/CACNT film is smaller than the K_M^{app} values reported at other CAT modified electrodes (Zhou et al., 2008; Salimi et al., 2007b). The smaller K_M^{app} value at CAT/CACNT film indicates its high affinity towards H_2O_2.

Fig. 5B displays the amperogram recorded at CAT/CACNT modified RDE in N_2 saturated PBS for various IO_3^- concentration additions. CAT/CACNT film exhibits steady, well defined amperometric response towards iodate within 4 s. In the calibration plot, the linear regression equation is I (mA) = 0.3216C (mM) + 3.5178, R^2 = 0.9394 (inset (a) in Fig. 5B). The linear concentration range and sensitivity values are 0.01–2.16 mM, and 0.253 mA mM^{-1} cm^{-2}, respectively. From the inset (b) in Fig. 5B, the slope, intercept, I_{max} and K_M^{app} values are 0.3216, 3.5178, 0.2843 and 0.09 mM, respectively. The smaller K_M^{app} value indicates high affinity of the CAT/CACNT film towards iodate.

The selectivity of the developed CAT/CACNT film towards 10 mM of H_2O_2 and 0.1 mM of iodate has also been investigated using amperometry and the results are shown in Fig. S9. As shown in Fig. S9(A), 10 mM of AA, DA and UA does not produce any interfere effect on the H_2O_2 reduction signals. Similarly, 0.1 mM of NO_2^-, DA and UA also does not produce any interference effect on the iodate reduction signals, which shows the excellent selectivity of the composite film for H_2O_2 and iodate (Fig. S9(B)).

3.7. Storage stability and repeatability studies

The CAT/CACNT film maintains the redox peaks at same position and it retains 95.03% of reduction peak current after 1 week storage in PBS at 4 °C which validates the good storage stability of composite film. The stability of this biosensor is attributed to the good stability of CACNT and the high affinity between CAT and CACNT films. Moreover, the relative standard deviation (RSD) for eight repetitive measurements of 1 mM H_2O_2 and 5 mM iodate at the composite film is 2.8% and 3.62% which validates the good repeatability of the proposed method for H_2O_2 and iodate quantifications.

4. Conclusions

We prepared a highly stable MWCNT aqueous dispersion using carminic acid as a novel dispersing agent. The prepared CACNT aqueous dispersion is highly stable for 4 months. For the first time, we utilized the CACNT matrix for immobilizing CAT to explore its direct electrochemistry. The excellent conductivity of CACNTs helps to achieve rapid direct electron transfer between the immobilized CAT and the electrode surface. The proposed CAT/CACNT biosensor exhibits high affinity, good selectivity, high sensitivity and appreciable anti-interference ability at physiological pH. Thus CACNT could be used as an effective platform for immobilizing vital proteins and biomolecules to explore their direct electrochemistry.

Appendix A. Supplementary data

Supplementary data associated with this article can be found, in the online version, at doi:10.1016/j.bios.2011.08.010.

References

Ahad, F., Ganie, S.A., 2010. Ijem 14, 13–17.
Ardakani, M.M., Moosavizadeh, S.H., Sadeghiane, A., Mashhadizadeh, M.H., 2010. Turk. J. Chem. 34, 229–240.
Bichsel, Y., Gunten, U.V., 1999. Anal. Chem. 71, 34–38.
Canamares, M.V., Ramos, J.V.G., Cortes, C.D.S.S., 2006. Vib. Spectrosc. 40, 161–167.
Carbo, A.D., Carbo, M.T.D., Peris, M.C.S., Adelantado, J.V.G., Reig, F.B., 2003. Anal. Bioanal. Chem. 375, 1169–1175.
Gaweda, S., Stochel, G., Szacilowski, K., 2008. J. Phys. Chem. C 112, 19131–19141.
Grygar, T., Kuckova, S., Hradil, D., Hradilova, D., 2003. J. Solid State Electrochem. 7, 706–713.
Heald, C.G.R., Wildgoose, G.G., Jiang, L., Jones, T.G.J., Compton, R.G., 2004. Chem. Phys. Chem. 5, 1794–1799.
Jackson, A.V., Hewitt, C.N., 1996. Atmos. Environ. 30, 819–830.
Kamin, R.A., Willson, G.S., 1980. Anal. Chem. 52, 1198–1205.
Kazuaki, I., 1997. Anal. Chem. 69, 3628–3632.
Ketpichainarong, W., Jittam, P., Ruenwongsa, P., Panijpan, B., 2010. J. Chem. Educ. 87, 662–664.
Kharisov, B.I., Kharissova, O.V., Gutierrez, H.L., Mendez, U.O., 2009. Ind. Eng. Chem. Res. 48, 572–590.
Kumar, A.S., Swetha, P., 2011. Colloids Surf. A: Physicochem. Eng. Aspects 384, 597–604.
Lancaster, F.E., Lawrence, J.F., 1996. J. Chromatogr. A 732, 394–398.
Laviron, E., 1979. J. Electroanal. Chem. 101, 19.
Li, Z., Wu, Z., Li, K., 2009a. Anal. Biochem. 387, 267–270.
Li, G.X., Liu, Z.Q., Wu, D., 2009b. J. Phys. Org. Chem. 22, 883–887.
Liu, A., Honma, I., Ichihara, H., Zhou, H., 2006. Nanotechnology 17, 2845–2849.
Lu, H., Rusling, J.F., Hu, N., 2007. J. Phys. Chem. B 111, 14378–14386.
Madni, I., Hwang, C., Park, S., Choa, Y., Kim, H., 2010. Colloids Surf. A: Physicochem. Eng. Aspects 358, 101–107.
Matsubara, C., Kudo, K., Kawashita, T., Takamura, K., 1985. Anal. Chem. 57, 1107–1109.
Moore, D.B., Argyropoulos, D.S., 1999. Anal. Chem. 71, 109–114.
Moulton, S.E., Minett, A.I., Murphy, R., Ryan, K.P., McCarthy, D., Coleman, J.N., Blau, W.J., Wallace, G.G., 2005. Carbon 43, 1879–1884.
Prakash, P.A., Yogeswaran, U., Chen, S.M., 2009a. Sensors 9, 1821–1844.
Prakash, P.A., Yogeswaran, U., Chen, S.M., 2009b. Talanta 78, 1414–1421.
Rashwan, F., 2005. Am. J. Appl. Sci. 2, 1595–1599.
Rasimas, J.P., Blanchard, G.J., 1995. J. Phys. Chem. 99, 11333–11338.
Salimi, A., Noorbakhsh, A., Ghadermarz, M., 2005. Anal. Biochem. 344, 16–24.
Salimi, A., Noorbakhsh, A., Ghadermarzi, M., 2007a. Sens. Actuators B 123, 530–537.
Salimi, A., Sharifi, E., Noorbakhsh, A., Soltanian, S., 2007b. Biophys. Chem. 125, 540–548.
Shen, L., Hu, N., 2004. Biochim. Biophys. Acta 1608, 23–33.
Shen, L., Hu, N., 2005. Biomacromolecules 6, 1475–1483.
Shima, S., Sordel-Klippert, M., Brioukhanov, A., Netrusov, A., Linder, D., Thauer, R.K., 2001. Appl. Environ. Microbiol. 67, 3041–3045.

Slesak, I., Libik, M., Karpinska, B., Karpinska, S., Miszalski, Z., 2007. Acta Biochim. Pol. 54, 39–50.
Srivastava, D., Wei, C., 2003. Appl. Mech. Rev. 56, 215–230.
Sun, W., Han, Y., Jiao, K., 2006. J. Serb. Chem. Soc. 71, 385–396.
Tasis, D., Tagmatarchis, N., Bianco, A., Prato, M., 2006. Chem. Rev. 106, 1105–1136.
Vatsyayan, P., Bordoloi, S., Goswami, P., 2010. Biophys. Chem. 153, 36–42.
Wang, Y., Wu, J., Wei, F., 2003. Carbon 41, 2939–2948.

Wang, S.F., Chen, T., Zhang, Z.L., Pang, D.W., Wong, K.Y., 2007. Electrochem. Commun. 9, 1709–1714.
Weston, R.J., 2000. Food Chem. 71, 235–239.
Yeh, C.K.J., Wu, H.M., Chen, T.C., 2003. J. Hazard. Mater. 96, 29–51.
Zarei, A.R., 2009. J. Anal. Chem. 64, 896–902.
Zhang, W., Silva, S.R.P., 2010. Scr. Mater. 63, 645–648.
Zhou, B., Wang, J., Gao, X., Tian, Y., 2008. Anal. Lett. 41, 1832–1849.